1962-06

Observations of large scale ionospheric irregularities as deduced from satellite information

Chisholm, George E.

Pennsylvania State University

The Pennsylvania State University

The Graduate School

Department of Physics

Observations of Large Scale Ionospheric Irregularities as Deduced from Satellite Information

A thesis in

Physics

by

Lieutenant George E. Chisholm II, U. S. Navy

Submitted in partial fulfillment
of the requirements
for the degree of

Master of Science

June 1962

The Pennsylvania State University

The Graduate School

Department of Physics

Observations of Large Scale Ionospheric Irregularities as Deduced from Satellite Information

A thesis in

Physics

by

Lieutenant George E. Chisholm II, U. S. Navy

Submitted in partial fulfillment
of the requirements
for the degree of

Master of Science

June 1962

Approved:

_____ _____

Associate Professor of Electrical Engineering,
Thesis Advisor

_____ _____

Head of the Department of Physics

ACKNOWLEDGMENTS

I wish to express my thanks to Dr. W. J. Ross for his suggestion of this problem and his patient guidance throughout the course of this work.

I further wish to express my appreciation to the other staff members, technicians, and computresses of the Ionosphere Research Laboratory for their assistance, and especially to Mrs. Nancy Barnes who carried out most of the computations involved in this work.

Appreciation is expressed to Mr. Guy Worsley of the Applied Physics Laboratory of the Johns Hopkins University for his assistance in providing a satellite ephemeris and the dispersive doppler records recorded at APL.

This work was carried out through the sponsorship of the U. S. Naval Postgraduate School, Monterey, California, and has been supported by the National Aeronautics and Space Administration under Grant NsG-114-61.

TABLE OF CONTENTS

		Page
ACKNOWLEDGMENTS		ii
LIST OF TABLES		v
LIST OF FIGURES		vi
CHAPTER I.	INTRODUCTION	1
	1. The Earth's Ionosphere	1
	2. Methods for Measuring Electron Distribution	5
	3. Irregularities	6
	4. Statement of the Problem	7
CHAPTER II.	IDENTIFICATION OF IONOSPHERIC IRREGULARITIES	8
	1. Magneto-ionic Theory	8
	2. Phase Path Length	11
	3. Dispersive Doppler	16
	4. Stratified Ionosphere with an Irregularity	16
CHAPTER III.	INSTRUMENTATION	20
	1. Satellite Properties	20
	2. Receiving Equipment	21
	3. Analysis Equipment	24
CHAPTER IV.	ANALYSIS TECHNIQUES	31
	1. Dispersive Doppler Curve Method of Analysis	31
	2. Difference in Phase Path Length Curve Analysis Method	33
	3. Profiles of Irregularities	35

Page

CHAPTER V. EXPERIMENTAL RESULTS 40

1. Magnitude of Irregularities 40

2. Horizontal Dimensions of Irregularities 44

3. Motion of Irregularities 47

4. Height of Irregularities 50

CHAPTER VI. SUMMARY AND CONCLUSIONS 52

CHAPTER VII. SUGGESTIONS FOR FURTHER INVESTIGATION 54

BIBLIOGRAPHY 55

LIST OF TABLES

Page

Table I. Occurrence of Irregularities 41

Table II. Magnitudes and Dimensions of Irregularities . . . 45

LIST OF FIGURES

		Page
Figure 1	Altitude Profile of Electron Density	4
Figure 2	Geometry for a Spherically Stratified Ionosphere	13
Figure 3	Schematic Phase Path and Dispersive Doppler Effects	15
Figure 4	Schematic Phase Path and Dispersive Doppler Effects with an Irregularity	17
Figure 5	Receiving and Recording Equipment	22
Figure 6	Dispersive Doppler Frequency Analysis System	25
Figure 7	Dispersive Doppler Record Showing Irregularity	26
Figure 8	Dispersive Doppler Plot	28
Figure 9	Difference in Phase Path Length Plot	30
Figure 10	Dispersive Doppler Plots	32
Figure 11	Profile of an Irregularity	34
Figure 12	Difference in Phase Path Length Plot with Best Fitted Parabola	36
Figure 13	Profile of Multiple Irregularity	37
Figure 14	Dispersive Doppler Plot Showing Possible Cyclic Irregularity	49

CHAPIER I

INTRODUCTION

1. The Earth's Ionosphere

That region of the earth's upper atmosphere extending from about 50 km up to great heights, where free electrons exist in quantities sufficient to affect the propagation of radio waves, is known as the ionosphere.[1] Its existence as an electrically conducting region was first postulated in 1878 by Balfour Stewart to explain small daily geomagnetic variations at the earth's surface. Later, in 1902, Kennelly in America and Heaviside in England postulated independently the presence of an ionized region in the earth's atmosphere to explain Marconi's transmission of radio waves across the Atlantic. Proof of the ionosphere came in 1925 when Appleton and Barnett showed the existence of sky waves returning from the Kennelly-Heaviside layer by comparing the intensities of fading of signals received simultaneously on a loop and a vertical antenna. At the same time, Breit and Tuve in the United States showed that a transmitted radio pulse produced two or more pulses in a receiver separated from the transmitter by a few kilometers. Their conclusion was that the extra pulses were due to echoes from the ionosphere.

Originally the ionosphere was thought of as a number of discrete layers of ionization but today it is more nearly thought of as a continuum of ionization.[1] That region below 90 km is called the D region, that between 90 and 160 km the E region, and that above 160 km the F region.

The production of ionization in the atmosphere is caused mainly by ultra-violet and x-radiation from the sun.[1] As the radiation penetrates the atmosphere the gas density increases, thus more and more electrons are produced per unit volume. In this process, however, the radiation is absorbed until finally the intensity of the radiation decreases at a faster rate than the gas density increases. This in turn causes the production to decrease below some height.

The important gaseous constituents responsible for the ionization in the upper atmosphere are molecular nitrogen and oxygen, atomic oxygen and nitric oxide.[2]

Turning to the loss processes present, electrons can undergo recombination or attachment.[1]

Two types of recombination exist. The first, radiative recombination, is where an electron combines with a singly ionized positive ion, atomic or molecular, with the emission of a photon. The second, dissociative recombination, is where an electron combines with a positively ionized molecule resulting in the dissociation of the molecule into two excited atoms. Of the two processes, the latter predominates in the ionosphere.[1]

Attachment is a process whereby an electron becomes attached to a neutral atom or molecule giving off energy to form a negative ion. Attachment is possible to atomic and molecular oxygen. Once this negative ion has been formed, the electron may be detached again by collisions with other particles or by the impingement of a photon

upon the ion (photo-detachment).

Diffusion also affects the distribution of electrons in the ionosphere. Because of the electrostatic forces between the electrons and the ions, any appreciable space charge is prevented from being built up and the plasma diffuses as a whole.[1] The presence of the geomagnetic field further restricts diffusion in that it tends to prevent diffusion across the lines of force. This leads to the result that the diffusion coefficient for the plasma is proportional to $\sin^2 I$ where I is the geomagnetic dip angle.

The combined effect of the above processes is responsible for the distribution of electron density within the ionosphere. Where a peak in density occurs within a region, it is termed a layer and given the same letter designation as the region in which it occurs. The layers within the F region are so designated by F1 and F2 layer. These layers are formed as a result of the different absorption, attachment and recombination coefficients for the constituents which themselves are distributed in the atmosphere as a function of height.

Figure 1 shows an electron density height profile computed from a rocket flight.[3] It can be seen here that the electron density increases to a maximum value at about 260 km. This corresponds to the peak of the F2 layer.

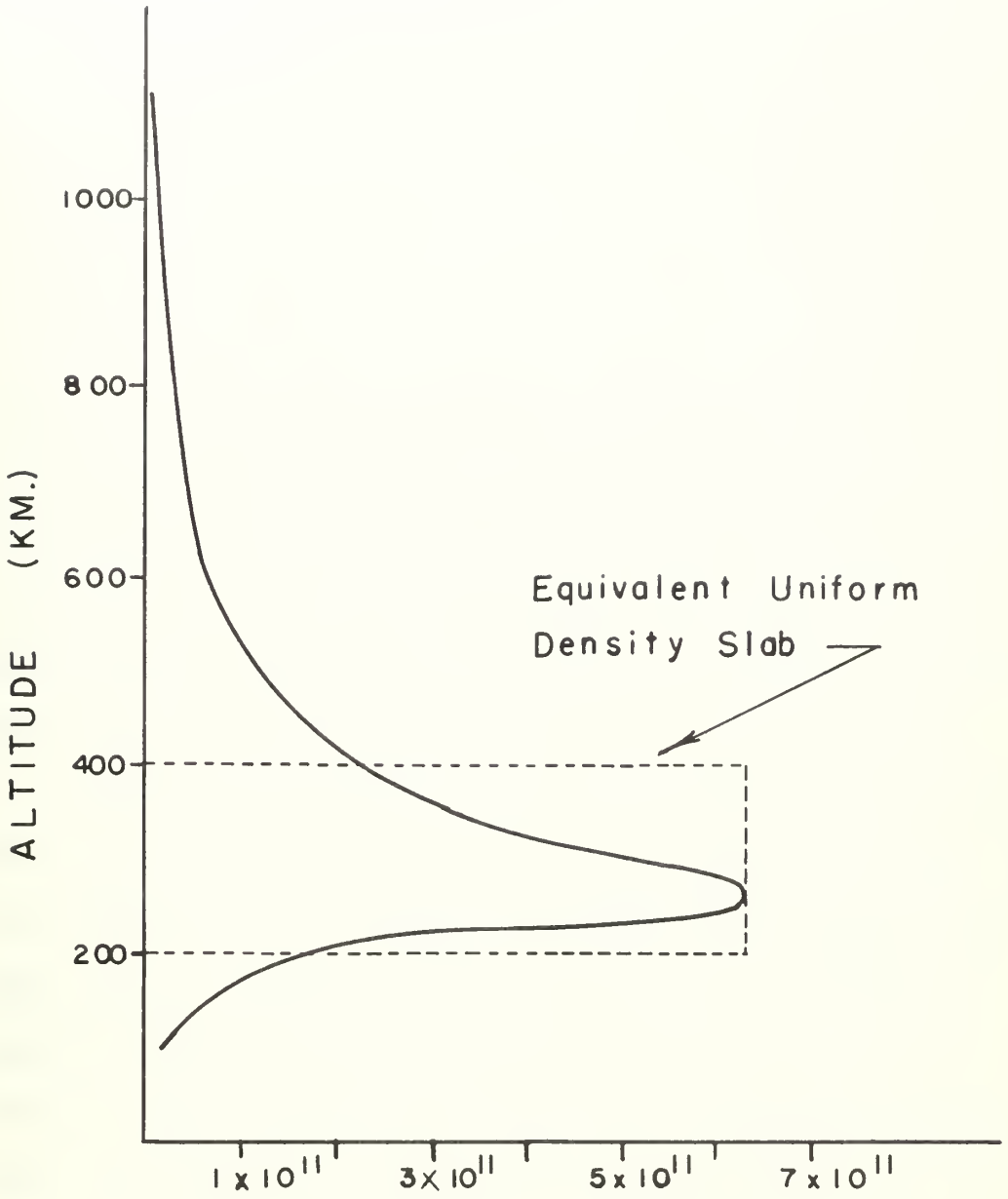

ALTITUDE PROFILE OF ELECTRON DENSITY

FIGURE 1

2. Methods for Measuring Electron Distribution

The most widely used method for determining the electron distribution in the ionosphere is vertical pulse sounding. This consists of transmitting upward pulses of radio waves whose carrier frequency is slowly varied. The time delay for the pulses to return to the ground is recorded as a function of carrier frequency. The equipment used here is known as an ionosonde and the record as an ionogram. The time delay is usually expressed as a virtual height, namely that height from which the waves would be reflected if they traveled at the speed of light for the interval of the time delay. The conversion of this virtual height to true height then becomes the problem in the reduction of ionograms into profiles of electron density as a function of height.

Methods have been developed for the reduction of ionograms.[4] The resulting profiles are limited, however, to extend in height only up to where the electron density is maximum in the F region. As a radio pulse is transmitted upward, it will be reflected when the plasma frequency, dependent upon the square root of the electron density, equals the frequency of the pulse. The maximum plasma frequency occurs when the electron density is the greatest at the peak of the F2 layer as shown on Figure 1. Any frequency higher than this will be transmitted through the ionosphere causing the limitation on the ionogram information. In order to overcome this difficulty, topside sounder experiments have been proposed using satellites which would sound the ionosphere from above the height

of peak density.

Propagation and probe methods have been used in conjunction with rockets and satellites to measure the electron distribution in the ionosphere. The probe methods sample the ionosphere immediately surrounding the satellite or rocket. The Langmuir probe technique[5] measures the current collected by a probe as a function of the probe potential. From this the electron density and temperature are calculated. Another method relates the electron density to the change of impedance of a probe.[6] Rocket measurements can yield a complete profile of the ionosphere up to the maximum altitude of the rocket[3] while some of the satellite techniques can only give the total columnar electron content up to the satellite height.[7]

Still a further technique for electron density measurements is the incoherent backscatter method[8] which employs the use of frequencies well above the plasma frequency. The power returned from any height is proportional to the electron density and inversely to the square of the range.[9] This method is not limited, as the vertical pulse sounder, to the region below the F2 electron peak and further it provides unambiguous results in valleys between layers.

3. Irregularities

The main production method in the ionosphere is from the sun's radiation as discussed in Section 1 of this chapter. This radiation illuminates almost uniformly a large region of the ionosphere at any given time causing the ionosphere to be basically stratified.

Experimental evidence shows, however, that irregularities do occur. Certain ones that occur only at night have been identified from the fading of radiation from radio stars in conjunction with diffraction theory.[10] These irregularities on the whole are elongated along the direction of the earth's magnetic field. Their dimension is of the order of five kilometers.[10]

Ionosondes have also been used to identify irregularities. One form, known as spread F, causes an echo from the F region to be much longer in duration than the incident pulse. It occurs mainly at night and is closely associated with geomagnetic activity.[11]

Another type of irregularity that causes cusps to appear on ionogram traces is attributed to horizontal traveling disturbances[12] which travel over distances as great as 3000 km.[13] Their extent can be greater than 1000 km.[13] Velocities for these disturbances have been measured at 1450 to 2750 km/hr[14] and also as low as 300 to 600 km/hr.[12] Explanations for these traveling waves have been proposed[15] yet none appears entirely satisfactory.[1]

4. Statement of the Problem

This thesis is concerned with the identification of large scale ionospheric irregularities deduced from radio signals received at University Park, Pennsylvania (40.79°N, 77.86°W) from earth satellite Transit 4A (1961 Omicron One). A technique for the analysis of the satellite records is developed and the results thereof are presented and discussed.

CHAPTER II

IDENTIFICATION OF IONOSPHERIC IRREGULARITIES

1. Magneto-ionic Theory

Wave propagation of electro-magnetic waves through a medium such as the ionosphere is explained by the magneto-ionic theory.[16] This medium is considered as one in which free electrons and heavy positive ions are distributed in a uniform magnetic field such that there is no resultant space charge. As the electric field of a wave moves through the medium it causes the electrons to oscillate setting up a radiation field which contributes to the overall electric field. This makes the medium appear to have a complex dielectric constant different from the free space value. The imaginary part of this constant is due mainly to collisions between the electrons and the heavier particles. Combining the effects of the magnetic field with the above leads to the Appleton-Hartree equation[16]

$$n^2 = 1 - \frac{X}{1 - iZ + 1/2 \dfrac{Y_T^2}{(1-X-iZ)} \pm \left[1/4 \dfrac{Y_T^4}{(1-X-iZ)} + Y_L^2 \right]^{1/2}} \qquad (1)$$

where n = complex refractive index $= \mu - i\chi$,

μ = refractive index,

χ = absorption index,

$$X = \frac{4\pi Ne^2}{\epsilon_o m \omega^2},$$

$$Y_T = \frac{\mu_o H_o e}{m\omega} \sin\theta ,$$

$$Y_L = \frac{\mu_o H_o e}{m\omega} \cos\theta ,$$

$$Z = \frac{\nu}{\omega} ,$$

N = free electron density,

e = the electronic charge,

m = the electronic mass,

ϵ_o = the electric permittivity of free space,

μ_o = the magnetic permittivity of free space,

H_o = the magnitude of the earth's magnetic field,

θ = the angle between the magnetic field vector and the direction of propagation,

ω = the angular wave frequency,

ν = the frequency of collision of electrons with heavy particles.

All quantities in the above are expressed in unrationalized units.

For those heights where the number of electrons is significant, the collision frequency ν is much smaller than the operating frequency. The term Z in equation (1) is neglected therefore. This means that it is assumed that the electrons will be able to travel large distances without colliding with heavier particles which further means that absorption of the electromagnetic waves in the medium is not present.

Equation (1) then reduces to:

$$\mu^2 = 1 - \frac{X}{1 + 1/2 \frac{Y_T^2}{(1-X)} \pm \left[1/4 \frac{Y_T^2}{(1-X)} + Y_L^2 \right]^{1/2}} \qquad (2)$$

For the frequencies of 54 mc/s and 324 mc/s used in this experiment, X will not exceed about .05 and the maximum value for Y_T and Y_L will be .025. Looking at the right hand term in the denominator of equation (2), Y_T enters to the fourth power while Y_L enters only to the second power, thus Y_L will be the dominant term except when X is close to unity or θ is close to $\frac{\pi}{2}$. As mentioned above X never gets close to unity and since the magnetic dip at University Park is about 72°, θ should never get close to $\frac{\pi}{2}$ over the region of interest which is around the observer's zenith. Finally since Y_L is much less than unity it is convenient to approximate the refractive index by the equation for no magnetic field

$$\mu^2 = 1 - X \qquad (3)$$

Since X is much less than unity a further approximation of equation (3) is possible by expanding μ in a binomial expansion and retaining the first two terms. This leads to the result

$$\mu \doteq 1 - \frac{\alpha N}{f^2} \qquad (4)$$

where $\alpha = \frac{e^2}{2\pi\epsilon_o m}$ and f is the operating wave frequency.

2. Phase Path Length

The phase path length is given by the expression

$$P = \int_{\text{ray path}} \mu \, ds \tag{5}$$

where μ is the refractive index corresponding to the operating frequency and ds is the differential length measured along the ray connecting the observer and the transmitter in the satellite.

Considering the case of a satellite transmitting 54 mc/s and 324 mc/s, the difference in phase path length between the two signals transmitted, expressed in cycles, can be written as

$$\Delta P = P_{324} - P_{54} = \frac{1}{\lambda_{324}} \int_{\text{ray path}} \mu_{324} \, ds - \frac{1}{\lambda_{324}} \int_{\text{ray path}} \mu_{54} \, ds \tag{6}$$

where from equation (4)

$$\mu_{54} = 1 - \beta N \, , \tag{7}$$

$$\mu_{324} = 1 - \frac{\beta N}{36} \, , \tag{8}$$

$$\beta = \frac{\alpha}{(54 \times 10^6)^2} \, ,$$

λ_{324} = the wave length in meters at 324 mc/s.

Now consider the case of a stratified ionosphere with all the ionization contained in a slab of thickness τ. Figure 1 gives justification for this model by showing that most of the ionization in the ionosphere lies from about 200 to 500 km. An equivalent uniform density slab is shown on this figure. For this case the slab thickness is about 200 kilometers. Since the satellite techniques

used in this experiment are insensitive to the height distribution of the electrons and since the satellite, at heights of about 950 km, is above most of the ionization anyway, this model is further justified. Figure 2 shows the geometry of the model.

For such a model it is valid to first order to consider the ray paths for the 54 and 324 mc/s signals the same and to consider this ray path to be a straight line. This can be seen by comparing the true phase path length with the straight line phase path length considering the effects of the ionosphere and with the straight line phase path length without the ionosphere. For an extreme case the above comparison shows that the difference between the true path and the approximate straight line path is less than 1% of the difference resulting from the presence of the ionosphere.

Substituting (7) and (8) in equation (6) and assuming straight line propagation yields

$$\Delta P = \frac{1}{\lambda_{324}} \int_{\text{ray path}} \left[\left(1 - \frac{\beta N}{36}\right) - \left(1 - \beta N\right) \right] ds = \frac{35}{36} \frac{\beta}{\lambda_{324}} \int_{\text{ray path}} N ds = \gamma \int_{\text{ray path}} N ds. \quad (9)$$

Over 97% of the contribution to (9) comes from the effect at 54 mc/s.

The zenith angle to the satellite measured at points along the ray is a function of height and will be designated as $\phi(h)$ where h is the vertical height to the point at which the angle is being measured. If dh is a differential vertical height then $ds = \sec\phi(h)\, dh$ for points along the ray. Substituting this expression for ds in equation (9) yields

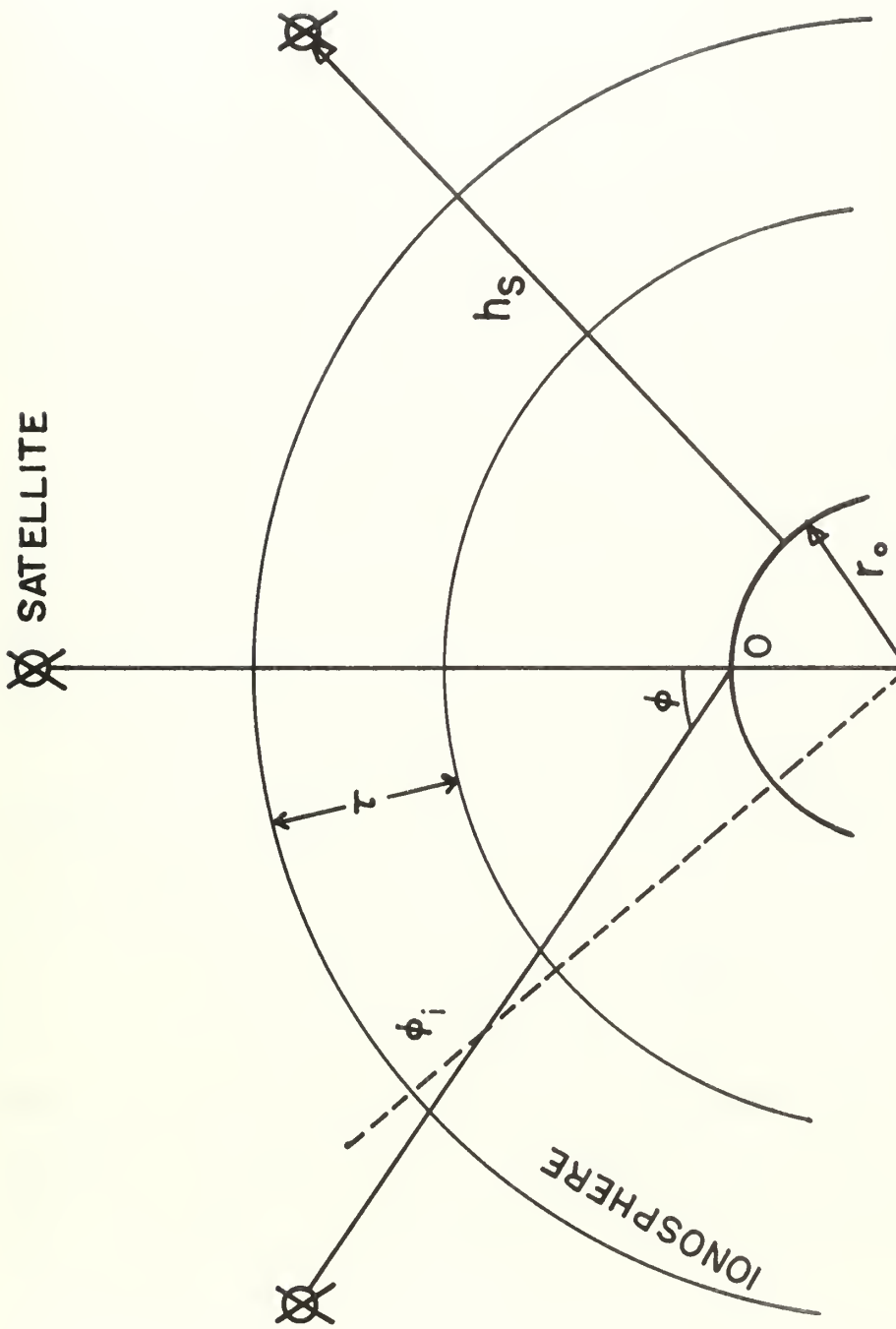

FIGURE 2

GEOMETRY FOR A SPHERICALLY STRATIFIED IONOSPHERE

$$\Delta P = \gamma \int_0^{hs} \sec \phi\,(h)\, N\, dh \tag{10}$$

where h_s is the height of the satellite above the ground. Contributions to the integral in (10) will occur only over the region of the ray that passes through the slab. Over this range sec ϕ (h) will be slowly varying and we can rewrite (10) as

$$\Delta P = \gamma\, \overline{\sec \phi} \int_0^{hs} N\, dh = \gamma\, \overline{\sec \phi}\, N_t \tag{11}$$

where $\overline{\sec \phi}$ is the mean average value of sec ϕ (h). The relation

$$\overline{\sec \phi} = \sec \phi_i \tag{12}$$

must hold therefore where ϕ_i is the zenith angle to the satellite measured along the ray at same point within the slab. In equation (11) N_t is the total number of electrons per square meter in a vertical column up to the satellite height.

Looking at Figure 2 it can be seen that ϕ_i can be related to ϕ, the zenith angle to the satellite measured from the observer O on the ground, by the relation

$$\phi_i = \sin^{-1}\left(\frac{r_o}{r_o + h_i} \sin \phi\right) \tag{13}$$

where h_i is the vertical height above the ground at which ϕ_i is measured. From equation (13), the maximum of ϕ_i occurs when $\phi = 90^o$ but never will ϕ_i reach 90^o itself, thus sec ϕ_i is always finite.

The top diagram on Figure 3 is a schematic drawing of a difference in phase path length vs. time curve. This curve will be

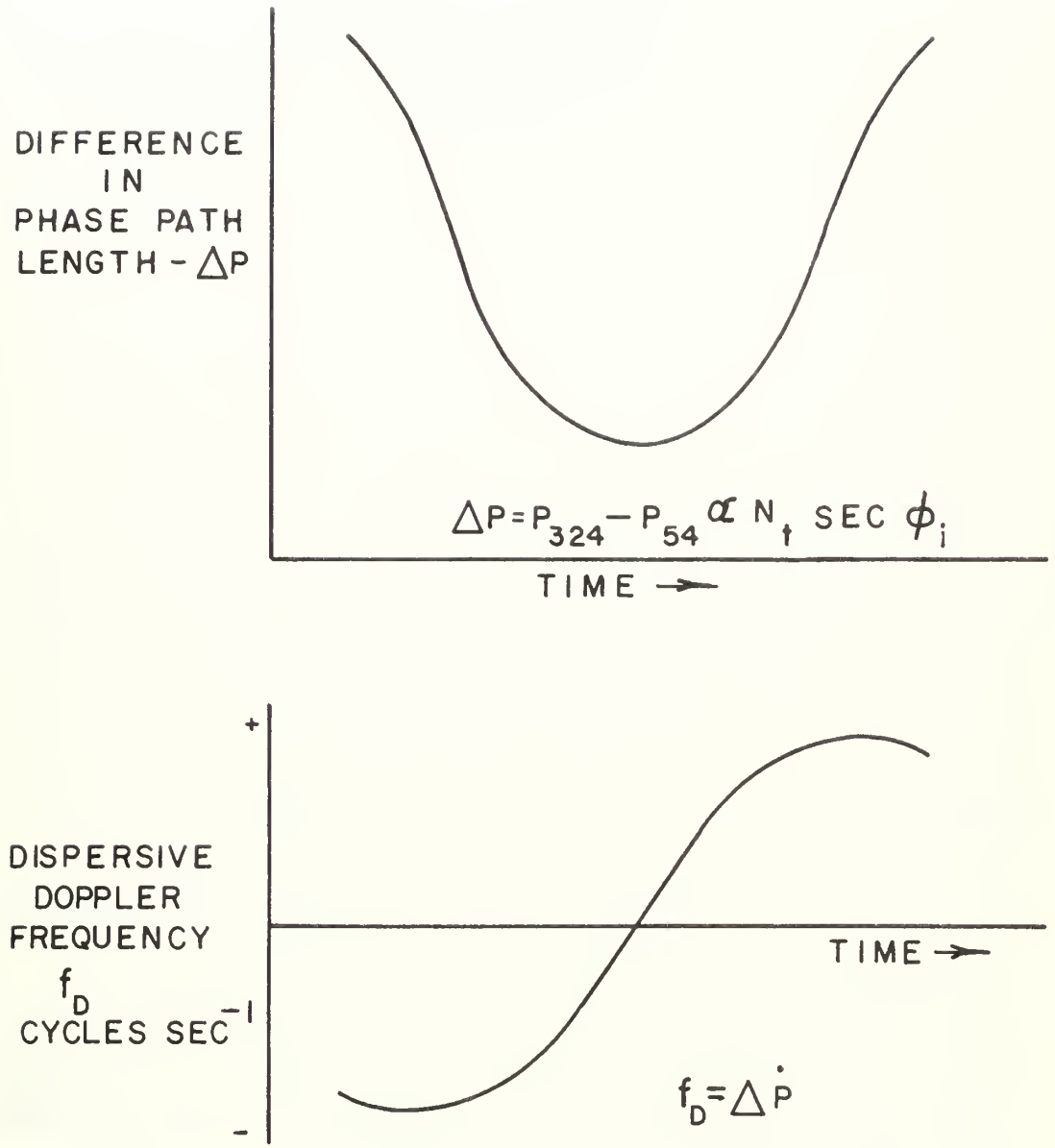

SCHEMATIC PHASE PATH AND DISPERSIVE DOPPLER EFFECTS

FIGURE 3

referred to as a normal difference in phase path length curve. If the satellite has a constant horizontal velocity this curve becomes an even function of time. As can be seen from equation (9), the minimum of this curve occurs when the total number of electrons along the ray from the observer to the satellite is a minimum.

3. Dispersive Doppler

Taking the derivative of the normal difference in phase path length curve with respect to time gives the frequency vs. time curve shown on the bottom of Figure 3. This dispersive doppler frequency, as it is called, is the difference frequency from a harmonic relation between the two received frequencies caused by the dispersive effects in the ionosphere. It can be measured experimentally as discussed in Chapter III and is a measure itself of the total columnar electron content up to the satellite height.[17]

4. Stratified Ionosphere with an Irregularity

Consider the case of a stratified ionosphere with an irregularity, corresponding to a region of excess ionization, superimposed thereon. The geometry of this situation is schematically represented in the top diagram of Figure 4. The thickening of the slab from A to B represents the irregularity and for this model means that either the density has remained unaltered over the region and the slab has thickened or the slab thickness has remained constant and the density has increased or some combination of these two effects.

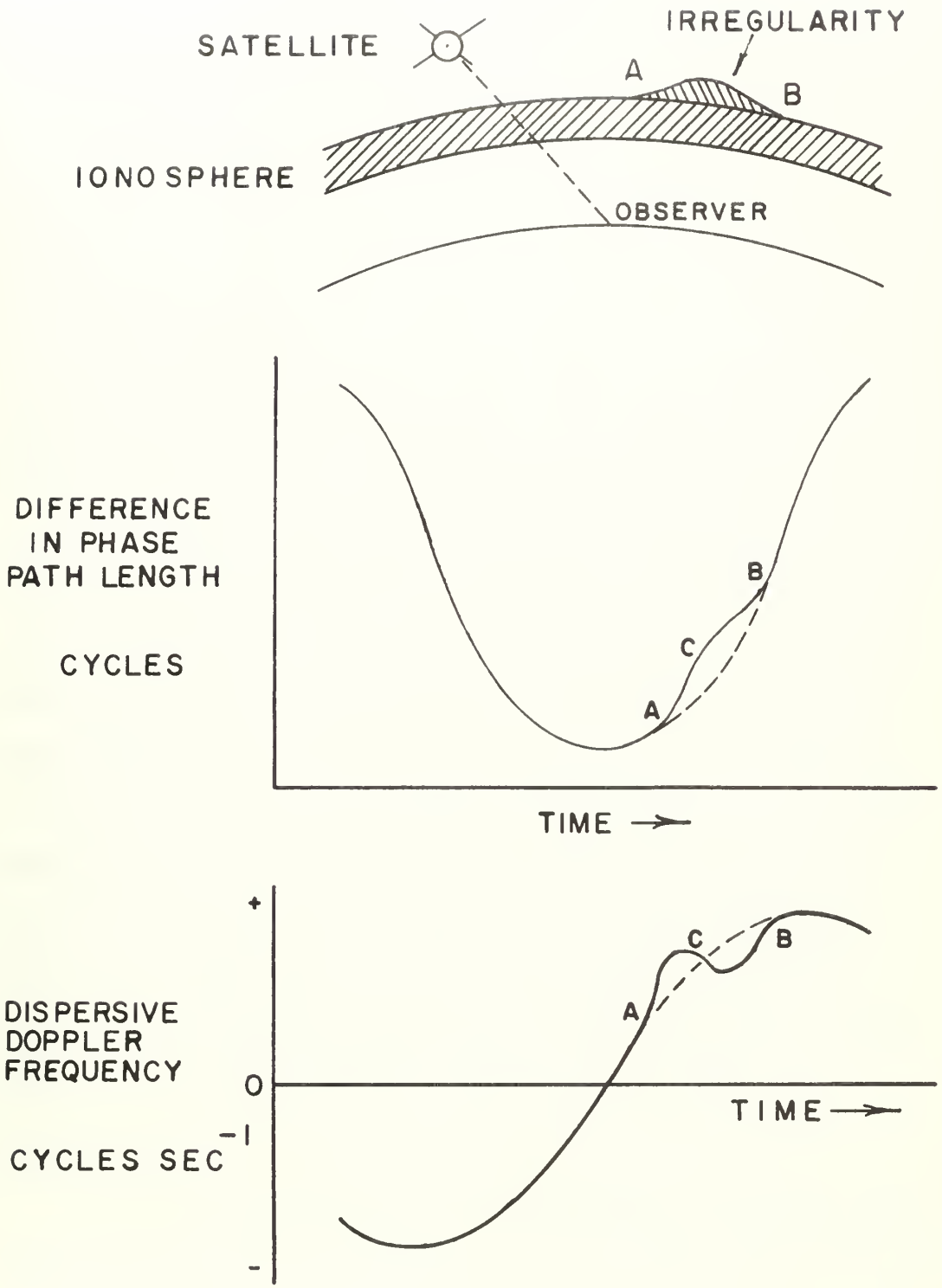

SCHEMATIC PHASE PATH AND DISPERSIVE DOPPLER EFFECTS WITH AN IRREGULARITY

FIGURE 4

For such a geometry being considered here, the corresponding difference in phase path length curve will be the same as the normal one when the ray between the observer and the satellite is not within the region from A to B. When the ray does fall within this region, there will be more electrons along it than in the case of no irregularity resulting in an increase in the difference in phase path length when the irregularity lies between the satellite and the observer. The curve ACB on the middle diagram of Figure 4 reflects the above conclusions.

The derivative of this difference in phase path length curve with respect to time will only show a change from the normal case over the time interval from A to B. Examination of the phase path curve shows that with respect to the normal curve (dotted line from A to B) the slope at A is identical, then becomes more positive until some point C where it is identical again, and then becomes less positive until it finally is identical again at B. Thus the dispersive doppler curve on the bottom of Figure 4 is arrived at. This plot is essentially a normal curve with an oscillation superimposed thereon over that time span when the ray between the satellite and the observer passed through the irregularity.

If in the above analysis the irregularity had been chosen to represent a region deficient in electrons, the final result would yield a normal dispersive doppler curve with an oscillation, only this time the negative half-cycle of the oscillation would appear

first in time.

Since the equations used in this analysis were linear, the principle of superposition can be applied to multiple irregularities and only their combined effect would be seen on the resultant dispersive doppler plot. This could mean the presence of more than one oscillation on a dispersive doppler record.

CHAPTER III

INSTRUMENTATION

1. Satellite Properties

The receiving and recording equipment was designed to record the 53.998 mc/s transmission and its sixth harmonic from earth satellite Transit 4A (1961 Omicron One). This satellite was designed by the Applied Physics Laboratory of The Johns Hopkins University as one of a series of experimental satellites to provide an operational marine navigation system. The satellite was launched on 29 June 1961 with the following initial orbit properties:

Anomalistic Period	103.84 minutes
Inclination	66.81 degrees
Perigee	881 km
Apogee	999 km
Eccentricity	.00804

The plane of a satellite orbit is approximately fixed in space so that an observer on the ground will pass through this plane twice each sidereal day due to the earth's axial rotation, if his latitude is less than the inclination of the orbital axis with the polar axis. The satellite orbit is not truely Keplerian, however, since the gravitational field of the earth is not truly central. This causes the orbit to precess in a sense opposite to that of the orbital motion. Combining this effect with the difference between solar and sidereal time gives the total observed precession.

In the case of Transit 4A the period of precession of the orbital plane about the earth is about three months. As a result of this there is a general trend backward in time for observing the satellite from day to day.

During the time it takes the satellite to make one revolution of its orbit, the earth will rotate a set amount and the plane of the orbit will precess. The combined effect of these for Transit 4A is to make the satellite cross the observer's latitude about 26° further west in longitude for each consecutive pass. This makes it possible to observe two consecutive satellite passes if neither crosses the observer's latitude with more than about 20° difference in longitude from the observer. Since, as stated earlier, the observer passes through the orbit plane twice each day, Transit 4A was observed on the average of three times daily.

The effective direction of travel for the satellite as observed from the ground at 40° N. latitude was about 152° true for south going passes and about 028° true for north going passes.

2. Receiving Equipment

Figure 5 is a block diagram of the receiving and recording equipment. The output from a voltage controlled oscillator near 1 mc/s is frequency multiplied by 54 and mixed with the 54 mc/s satellite signal received on a fixed crossed dipole antenna. Both signals are then converted in a crystal controlled converter at which point, after being amplified in a fixed-gain multiple-conversion crystal-controlled receiver, the difference between them

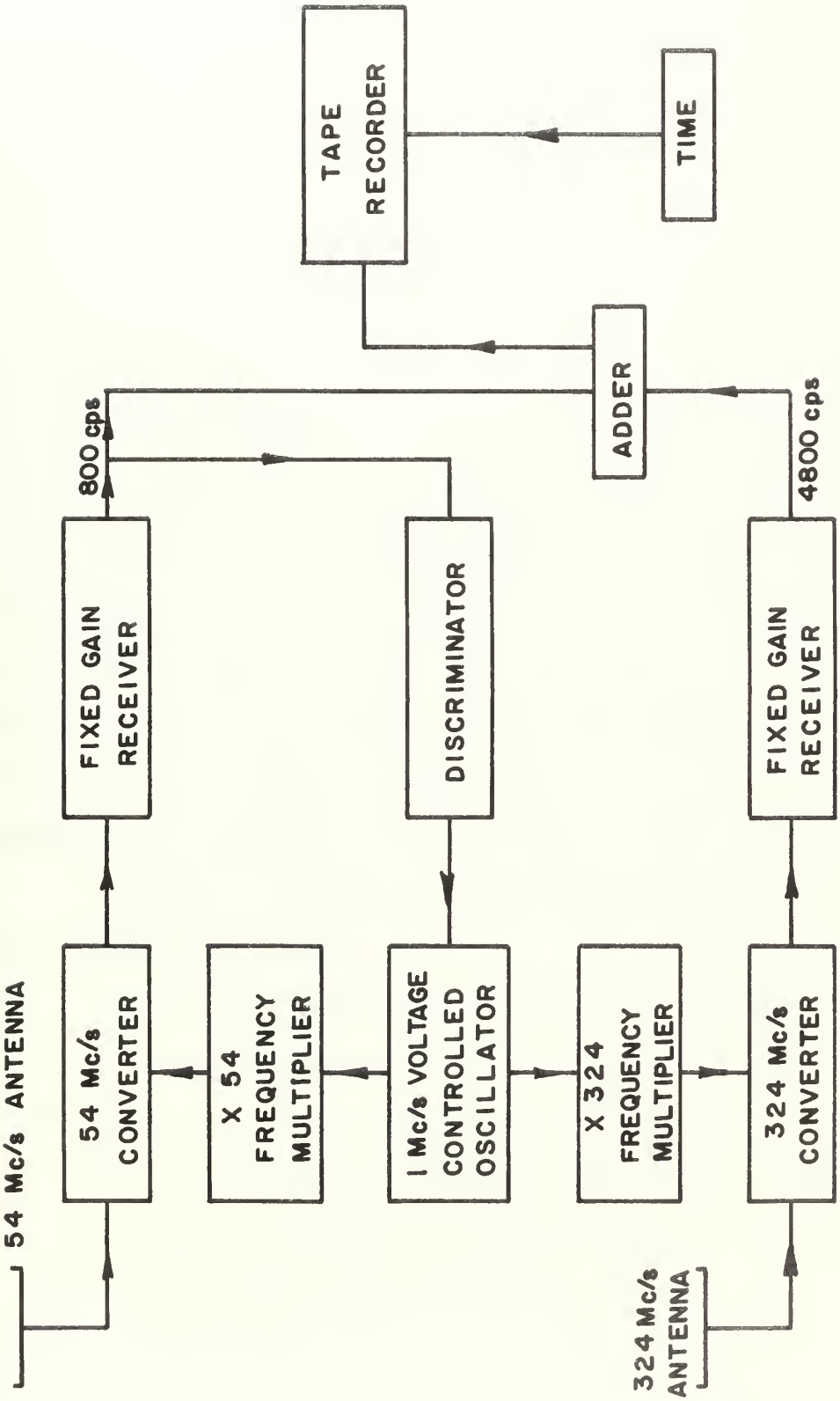

RECEIVING AND RECORDING EQUIPMENT

FIGURE 5

is detected. The intermediate frequency stages of the receiver have a bandwidth of 2.5 kc/s to accommodate the free space doppler shift on the 54 mc/s signal while the audio output stage has a bandwidth of only 100 cycles since the free space doppler shift has been removed.

The above detected difference controls a discriminator circuit which in turn controls the frequency of the voltage controlled oscillator. The discriminator is designed to detect the departure of this difference frequency from 800 cycles/s. If the difference frequency is greater than 800 cycles/s the resultant departure produces a voltage which reduces the frequency output of the voltage controlled oscillator. The reverse of this holds if the difference frequency is less than 800 cycles/s. As a result of the above a stable condition exists when the frequency of the signal from the voltage controlled oscillator is greater than the satellite frequency and an unstable condition exists when the reverse is true.

The 324 mc/s system is similar to the 54 mc/s system with the following exceptions:

a. The 324 mc/s signal is preamplified prior to going to the converter.

b. There is no discriminator in this system.

c. The intermediate frequency stages of the receiver have a bandwidth of 15 kc/s because of the increased free space doppler shift at 324 mc/s.

d. The bandwidth of the output stage of the receiver is 300 cycles/s.

e. The output frequency from the receiver is about 4800 cycles/s.

The 800 and 4800 cyles/s signals are added and recorded on a magnetic tape recorder. Other recorded quantities are the 54 mc/s and 324 mc/s signal amplitudes and time.

3. Analysis Equipment

Figure 6 is a block diagram of the analysis equipment. A filter separates the 800 and 4800 cycles/s signals. The former signal is then frequency multiplied by six and its phase is compared with the latter signal in two phase detectors as shown. The 4800 cycles/s signal to one detector has been shifted ahead in phase by 45^{o} and to the other detector has been shifted behind by 45^{o}. This quadrature relationship between the inputs allows discrimination of positive and negative dispersive doppler frequency.

The outputs shown on Figure 6 are: ① dispersive doppler frequency, ② quadrature dispersive doppler frequency, and ③ time. All of these quantities are recorded graphically with a Sanborn 358 graphic recorder using a normal chart speed of 10 mm/s.

A section of a chart showing only the two dispersive doppler channels is shown on Figure 7. This record corresponds to a satellite pass that occurred on 8 July 1961 at about 1123 eastern standard time. The chart speed used for this record was 2.5 mm/s.

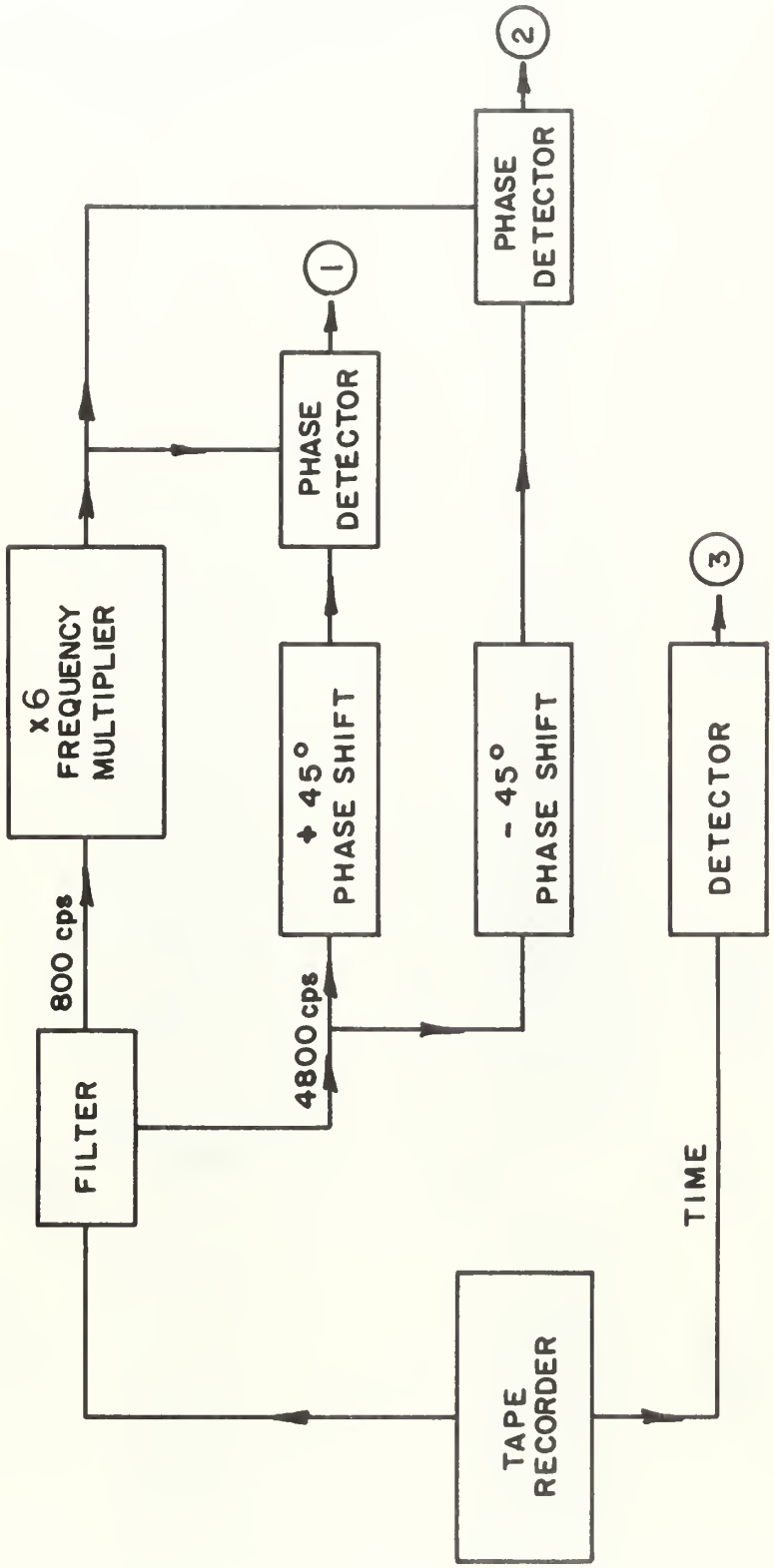

DISPERSIVE DOPPLER FREQUENCY ANALYSIS SYSTEM

FIGURE 6

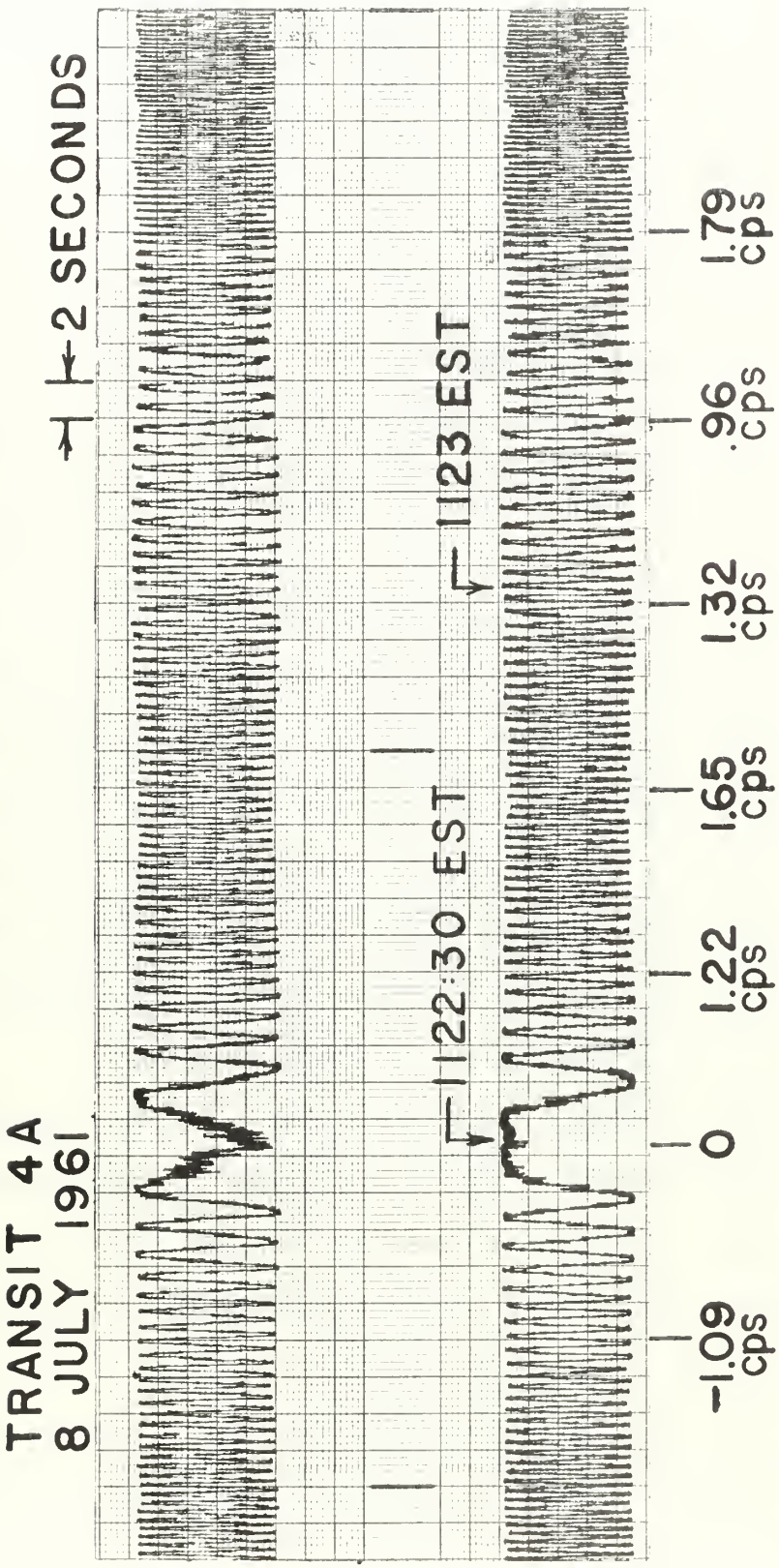

FIGURE 7

DISPERSIVE DOPPLER RECORD SHOWING IRREGULARITY

The dominant feature of this record is the clearly defined dispersive doppler zero to the left of center. To the left of this point the phase of the cycles on the upper trace leads the phase on the lower trace by ninety degrees while to the right of zero this condition is reversed. This allows the identification of positive and negative dispersive doppler frequency.

On the right hand side of this record the frequency drops from 1.32 cps to .96 cps and then rises to 1.79 cps. This effect corresponds to an irregularity in the ionosphere as postulated in Chapter II, Section 4.

Each cycle on the record corresponds to a change in the difference in phase path length for the two signals equal to one wave length measured at 324 mc/s. Expressed in electrons/m^2, this means that over the time interval of the cycle the number of electrons/m^2 along the ray from the satellite to the observer has changed by 6.8×10^{13} electrons/m^2. This conversion factor from cycles to electrons/m^2 comes from evaluation of γ in equation (9).

In order to plot such a record as this the frequency is averaged over ten-second intervals and plotted against the time corresponding to the mean of the time interval. This results in the dispersive doppler plot shown on Figure 8. Those points contained within the dashed rectangle correspond to the part of the dispersive doppler record shown on Figure 7. The ten second averaging used here smooths out small scale scintillations that are possibly caused by small irregularities.

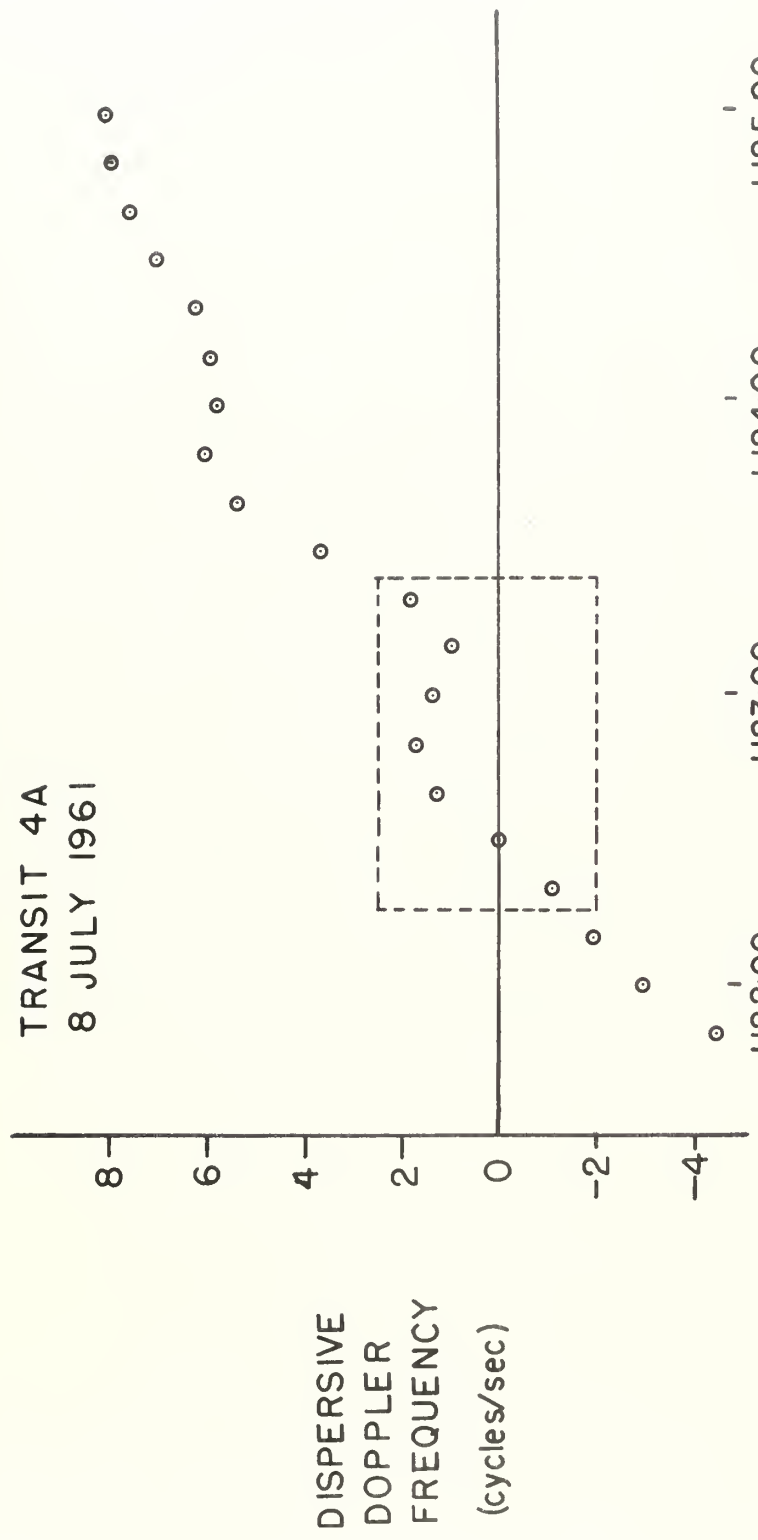

DISPERSIVE DOPPLER PLOT

FIGURE 8

An alternative method for plotting a dispersive doppler record is to start at dispersive doppler zero and count the total number of cycles to the left of this point, plotting the cumulative number of cycles from zero against the corresponding time at five-second intervals. Then follow the same procedure to the right of dispersive doppler zero. This method is applicable only to those records that are continuous, all the cycles are defined over some range on either side of the zero point. Figure 9 shows the plot of the record on Figure 7 using this method. It is a difference in phase path length curve which shows only relative differences between points since the integration of the frequency record introduces an unknown constant of integration. The constant equals the number of cycles corresponding to the total number of electrons/m^2 along the ray from the satellite to the observer at the time the difference in phase path length curve is a minimum. It is of the order of 3000 cycles while the range of the difference in phase path length curve is about 500 cycles on the average.

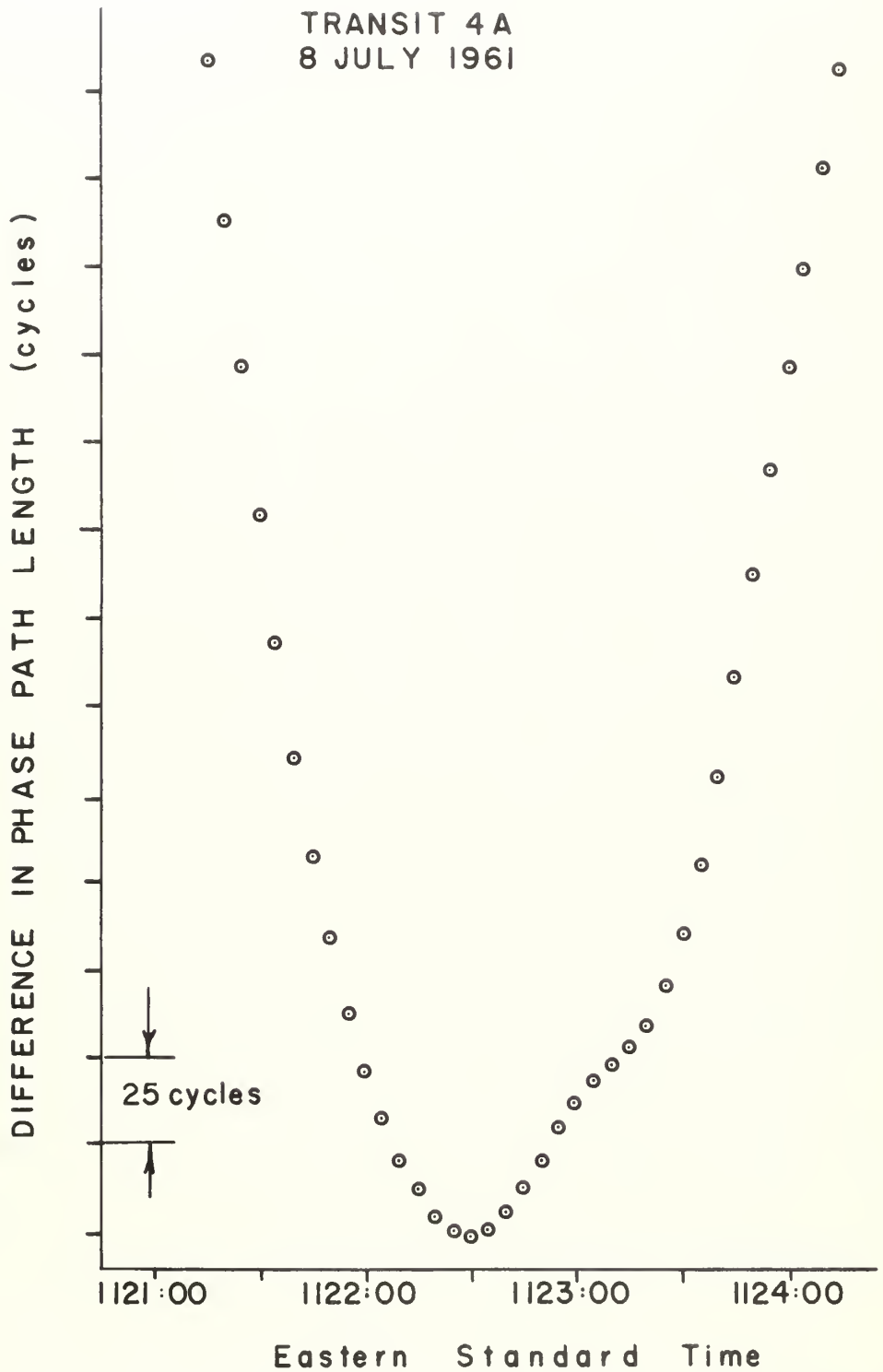

DIFFERENCE IN PHASE PATH LENGTH PLOT

FIGURE 9

.25 cycles

CHAPTER IV

ANALYSIS TECHNIQUES

Two methods were used to analyze those dispersive doppler curves that exhibited departures as postulated in Chapter II, Section 4. The first was applied to dispersive doppler curves while the second was applied to difference in phase path length curves.

1. Dispersive Doppler Curve Method of Analysis

Over the range of a satellite observation the corresponding dispersive doppler curve is essentially a straight line and the curvature of the ends, as shown on Figure 3 for the normal case, is seldom realized. The first step in analysis therefore was to fit the best straight line by least squares method to certain curves showing the presence of irregularities in the ionosphere. Since this line represents an ambient ionosphere from which departures are measured, the results of further analysis are dependent upon its location. Such a curve is shown on Figure 10 for a satellite pass that occurred on 24 October 1961 about 1000 eastern standard time. From D to E on this plot is a departure corresponding to an irregularity of excess ionization. As mentioned in Chapter III, Section 3, the points of this plot are ten second averages so that any scintillations of smaller order than this are smoothed over leaving only the larger scale irregularities.

Once the ambient line was fitted to the plot the next step was to integrate the dispersive doppler curve over the region of the

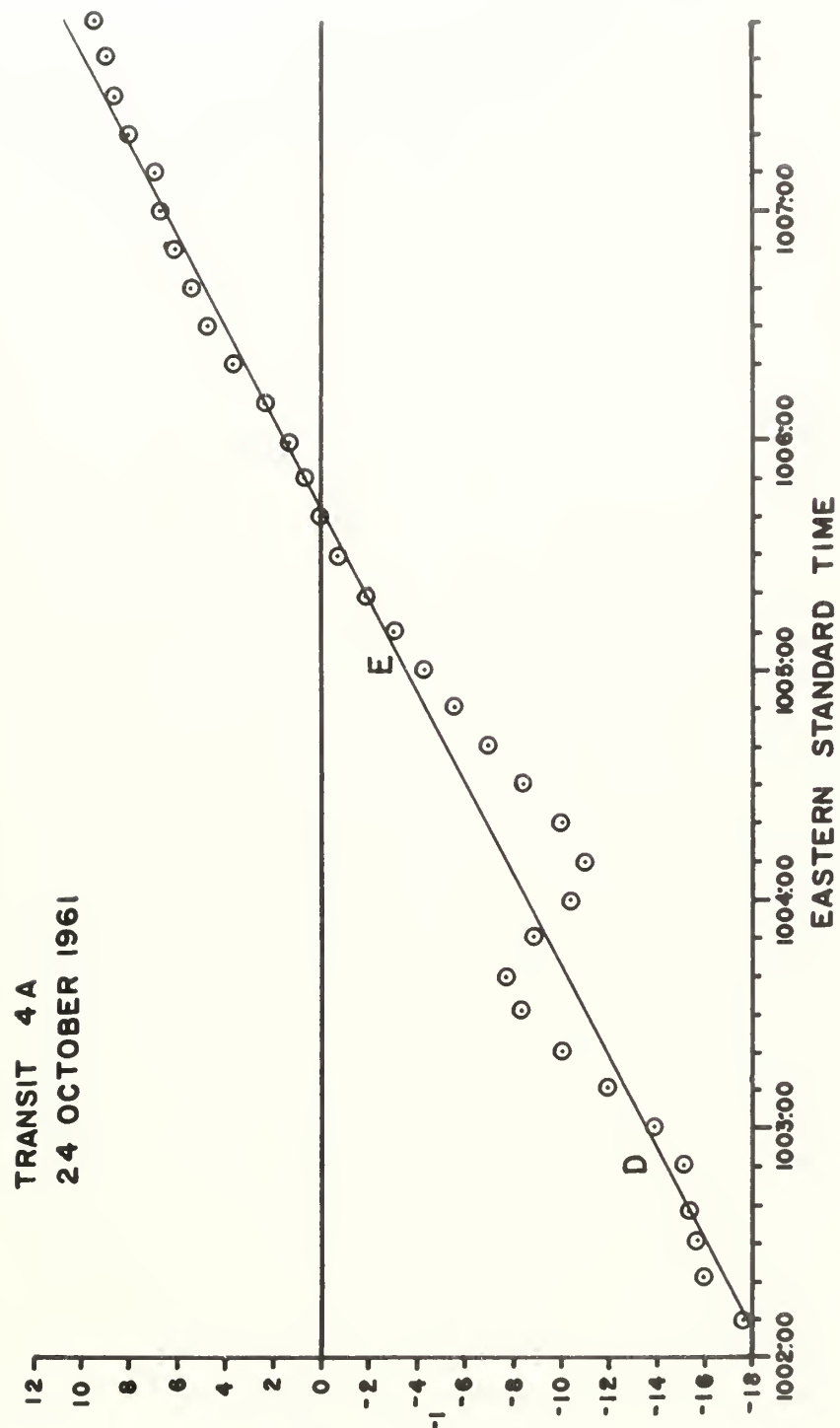

DISPERSIVE DOPPLER PLOT

FIGURE 10

irregularity with respect to this line. This yielded a profile plot for the irregularity in cycles vs. time. Figure 11 is the profile for the irregularity corresponding to the dispersive doppler plot on Figure 10.

2. Difference in Phase Path Length Curve Analysis Method

For those dispersive doppler records that were continuous (Chapter III, Section 3) and from which a difference in phase path length plot could be obtained, a different method of analysis was used.

To ideally represent the ambient ionosphere on such a plot would involve fitting a function to the experimental points that is proportional to the secant of the zenith angle to the satellite as measured in the ionosphere. This makes it necessary to know the zenith angle to the satellite as a function of time and also the unknown constant of integration discussed in Chapter III, Section 3. The former of these items can be obtained from knowledge of the satellite orbit, but even with knowledge of the total electron content there is some ambiguity as to the value of the constant and especially so when the phase path record is irregular.

An approximation was made to avoid this ambiguity. Since the satellite used in this experiment had a small vertical velocity compared with its horizontal velocity and since the horizontal velocity was almost constant for the duration of a given satellite pass, it seemed reasonable to assume that the difference in phase path length curve should be an even function of time. Also it turns

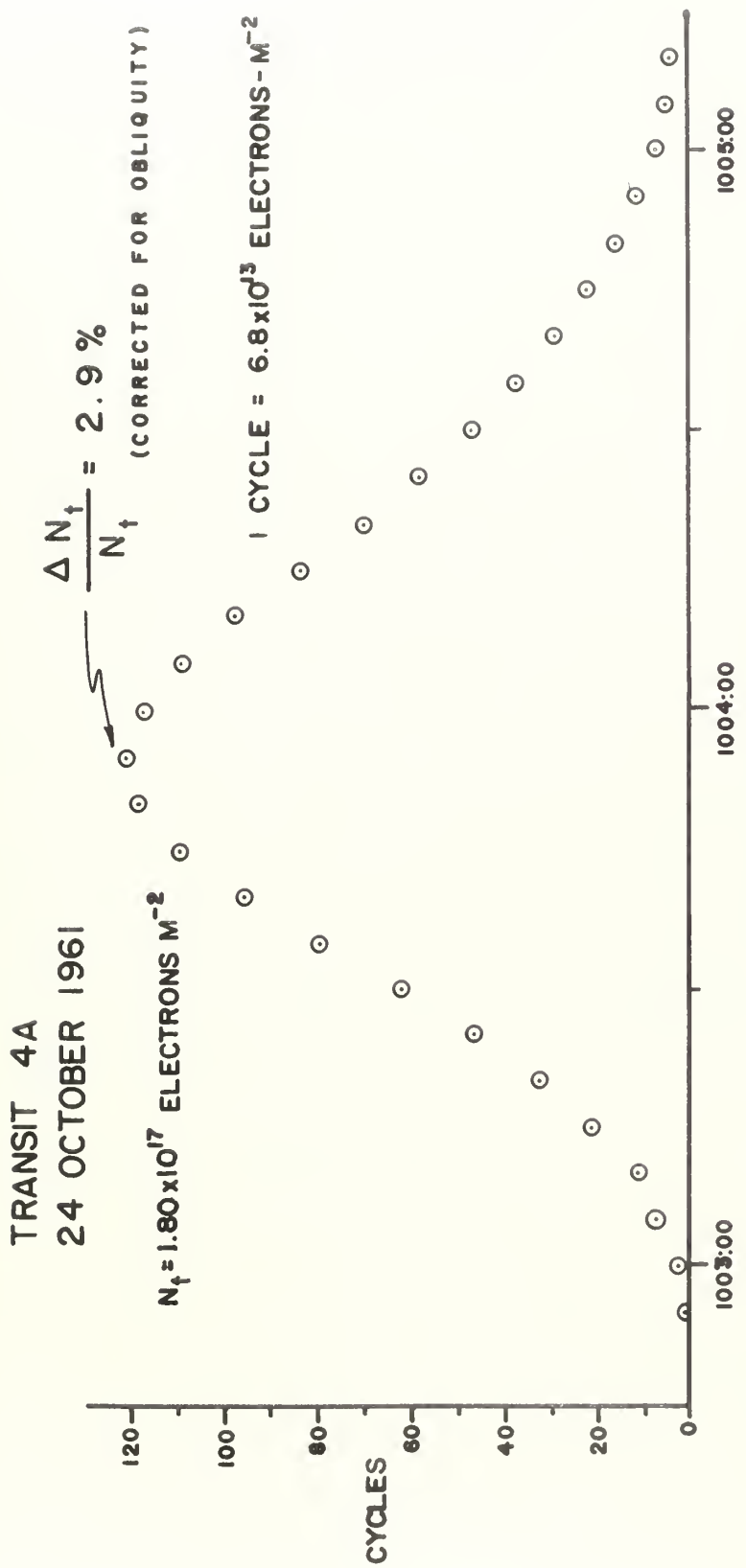

PROFILE OF AN IRREGULARITY

FIGURE 11

out experimentally that the outward bending of the ends of the phase path curve is not seen. In view of these factors the ambient ionosphere was approximated by a parabola thereby eliminating the need to know the satellite ephemeris and the constant of integration.

As with the case of fitting a straight line to dispersive doppler plots, there is some arbitrariness in assuming that a parabola, fitted by the method of least squares to the difference in phase path length plot, is the best approximation of the ambient ionosphere. In order to reduce this uncertainty the same restriction was placed on records for analysis by the parabola method as for those analyzed by the straight line method, namely only those records were used whose dispersive doppler curves fairly well defined a straight line as discussed previously in this chapter.

Figure 12 shows a difference in phase path length plot with a parabola fitted to the experimental points. The difference between these two curves yields a profile for the irregularities in terms of cycles vs. time. The profile corresponding to this record is shown on Figure 13.

3. Profiles of Irregularities

The above fitting of a parabola and straight line ambient directly affects the resultant profile plot. In certain cases the profiles had long extended tails. These were most apparent when trying to analyze a record by the parabola method when the irregularity was located near either end of the record. Such profiles were not used for further analysis. It should be noted also that a

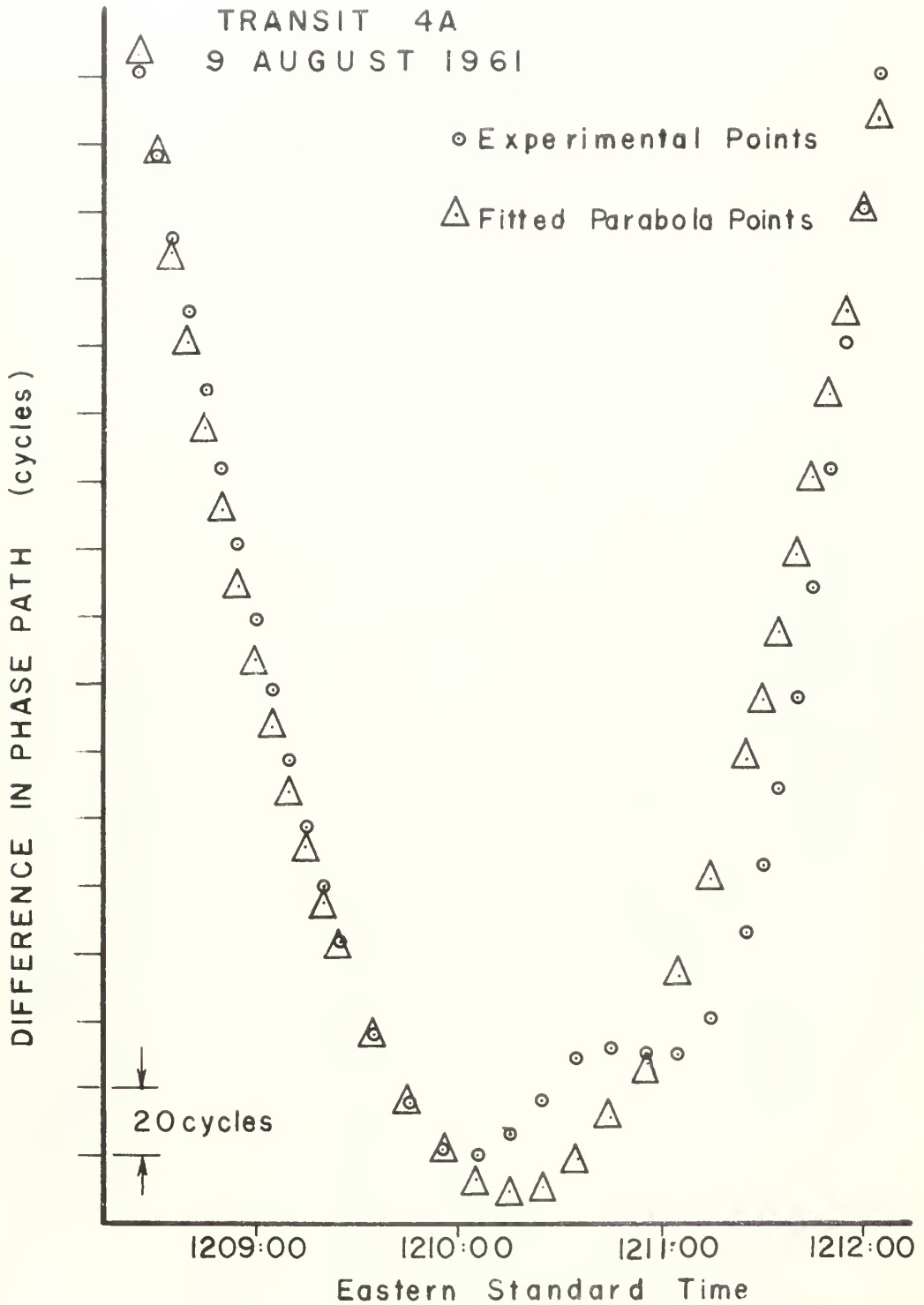

DIFFERENCE IN PHASE PATH LENGTH PLOT

WITH BEST FITTED PARABOLA

FIGURE 12

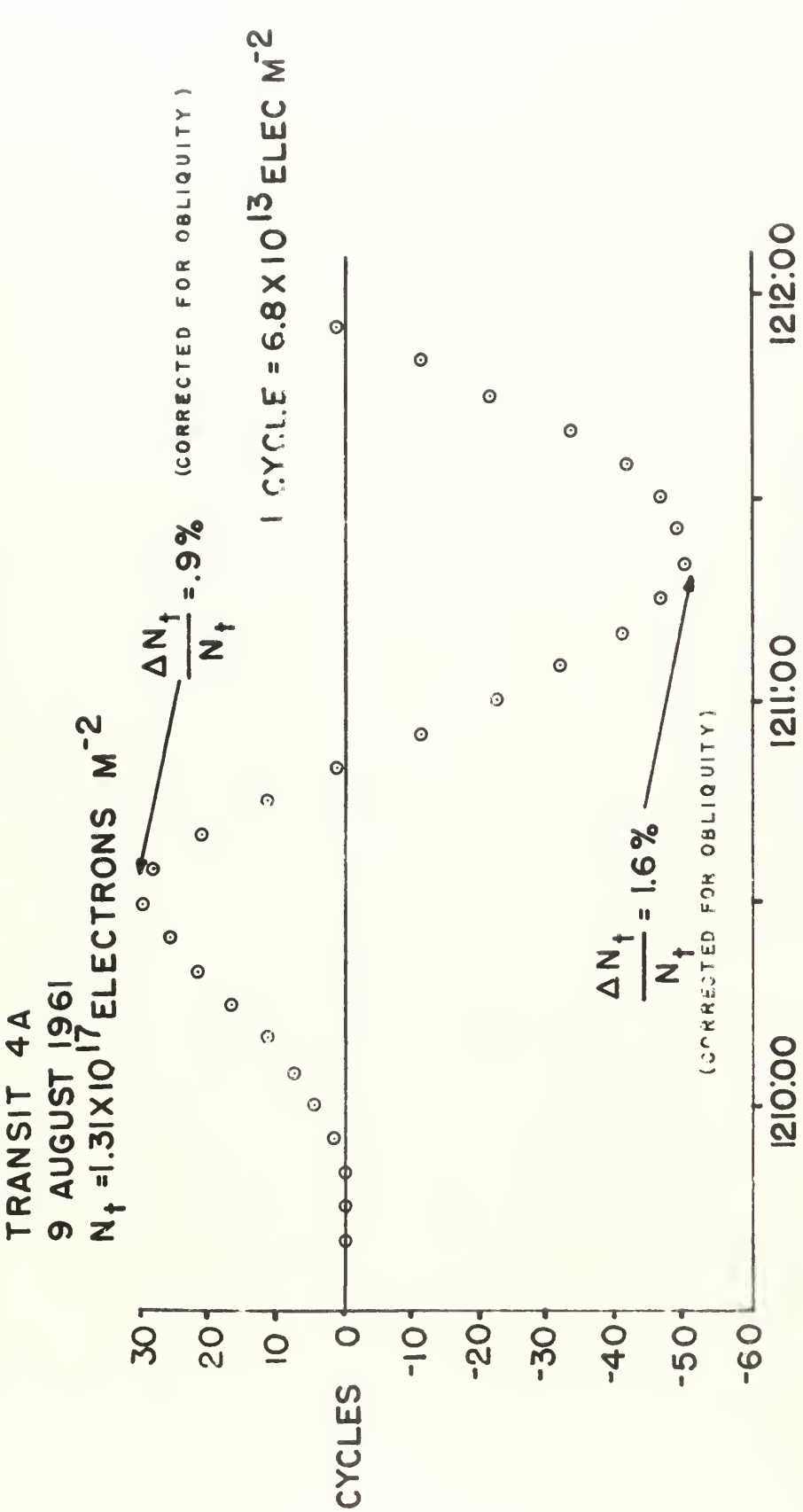

PROFILE OF MULTIPLE IRREGULARITY
FIGURE 13

vertical translation of a fitted parabola could possibly cause an irregularity of excess ionization to appear as an irregularity deficient in ionization.

Those profiles that were chosen for further analysis were utilized in two ways. Firstly, the peaks of the irregularities as expressed in cycles were converted into electrons/m^2 using the appropriate conversion factor that one cycle equals 6.8×10^{13} electrons/m^2. The new value for the peak was then expressed as a percent of the total columnar electron content up to the satellite height. The two values of the peak, one in electrons/m^2 and the other in terms of a percent of the total electron content, were corrected then for obliquity and the final values were used as a measure of the magnitude of the irregularity. This correction involved determining the zenith angle to the satellite measured from the location of the irregularity peak at an assumed height of 400 km. The cosine of this angle multiplied by the original value of the peak gives the corrected value.

The second use for the profile plots was in the determination of a horizontal dimension for the irregularities. Since the profile resulting from the dispersive doppler curve method of analysis strongly resembles a gaussian distribution, such a function was fitted to all the profiles and the one standard deviation points were located thereon as a standard of measurement.

Considering the case of a single irregularity, the ground track for the corresponding satellite pass was plotted on a conformal

grid using an ephemeris provided by The Applied Physics Laboratory. On such a grid straight lines represent great circles. Since the eccentricity of Transit 4A's orbit was small its ground track on the conformal grid was essentially a straight line. The times of the one standard deviation points were located on the satellite ground track and rays were drawn to these points from the observer. Using linear interpolation the points where the rays were at a height of 400 km were located. The distance between these points was used as a horizontal dimension for the irregularity. This dimension was measured in the surface traced out by the ray from the observer to the satellite. Over the range of an irregularity this surface was essentially a plane so that the measured dimension was parallel to the satellite ground track. If a height of 200 km had been chosen instead of 400 km the dimension would have been half of that as measured here.

The point, where the ray from the observer to the peak of the irregularity intersected the line joining the 400 km points on the rays, gave a location for the irregularity at 400 km height. This location was used to determine the zenith angle to the satellite, measured at the irregularity, which was needed for the obliquity correction to the irregularity magnitude as discussed earlier in this Section.

CHAPTER V

EXPERIMENTAL RESULTS

The data analyzed in this experiment covered the period from 29 June 1961 to 10 April 1962. During this period 501 dispersive doppler records were reduced of which 90 of them showed evidence of the presence of large scale ionospheric irregularities as postulated in Chapter II, Section 4. Table I shows that these irregularities occur at all times of day with over two-thirds of them occurring between the hours of 0800 and 1800 eastern standard time. This result is not surprising since the daytime records exhibit less scatter in general than do the night-time ones thereby making identification of irregularities easier during the day. It should also be noted that the irregularities as identified here are restricted both to those that occur at a time when the satellite is in view of the observer and to those that are in such a location that the ray from the observer to the satellite passes through them.

1. Magnitude of Irregularities

Using the methods described in Chapter IV, twenty-seven records were analyzed. Eleven of these had one region of excess ionization, two had one region deficient in ionization, nine had both an excess region and a deficient region, four had two excess regions, and one had a region of excess ionization and two deficient regions. This makes a total of forty-two irregularities that were analyzed.

Table I

Occurrence of Irregularities

Date	Time EST	Date	Time EST
7- 3-61	1156	9- 5-61	0613
7- 7-61	1108	9-18-61	0401
7- 8-61	1122	9-27-61	0240
7-10-61	1152	9-29-61	0120
7-15-61	0929	10- 5-61	2329
7-19-61	1030	10- 9-61	1335
7-19-61	1745	10-19-61	2130
7-23-61	0753	10-20-61	1055
7-24-61	1713	10-20-61	2147
7-28-61	1622	10-24-61	1003
7-29-61	1451	10-25-61	1017
8- 1-61	0630	10-26-61	1940
8- 5-61	1258	10-27-61	0901
8- 9-61	1210	10-30-61	1851
8- 9-61	1358	11- 4-61	1815
8-12-61	1106	11- 6-61	1658
8-13-61	1121	11- 8-61	1727
8-14-61	0230	11-19-61	1445
8-16-61	1018	11-26-61	1254
8-21-61	0945	11-27-61	1121
8-24-61	0113	11-28-61	1136
8-24-61	2350	12- 4-61	1116
8-25-61	0856	12-31-61	1842

Table I continued.

Date	Time Est	Date	Time Est
1- 1-62	1859	2- 2-62	1226
1- 4-62	1754	2- 3-62	1235
1- 7-62	1650	2- 3-62	2144
1- 7-62	1836	2- 6-62	2041
1- 8-62	1706	2- 7-62	1005
1- 9-62	1719	2- 7-62	1149
1-10-62	0224	2- 8-62	1018
1-11-62	1559	2-10-62	0900
1-11-62	1746	2-11-62	0915
1-12-62	1614	2-13-62	0942
1-16-62	1530	2-13-62	1846
1-18-62	1555	2-14-62	0958
1-20-62	1437	2-14-62	1904
1-23-62	1330	2-15-62	1732
1-24-62	2254	2-17-62	0854
1-27-62	1245	2-27-62	0600
1-27-62	1430	3- 2-62	0454
1-31-62	1153	3- 3-62	1414
1-31-62	1342	3- 3-62	1601
2- 1-62	1207	3- 5-62	1259
2- 1-62	2115	3- 6-62	1310
2- 2-62	1038	3-24-62	0841

The magnitude of the peak of these irregularities, in terms of percent of total electron content, ranged in value from .3% to 4.8%. The average value for the twenty-eight irregularities of excess ionization was 1.5% and the average value for the fourteen irregularities deficient in ionization was 1.2%, the overall average being 1.4%.

Figure 11 shows a profile whose peak represents an excess of ionization equal to 2.9% of the total electron content. Such a percentage represents a minimum value in that if at each height up to the satellite height the irregularity at its peak contained an excess of ionization equal to 2.9% of the local electron density then the overall peak would contain the necessary 2.9% of the total electron content. If on the other hand, however, the irregularity were restrained in height, then at some point the peak would have to contain more than 2.9% of the local density.

Expressing the magnitude of the peak of these irregularities in terms of electrons/m^2, the range of values now runs from $.18 \times 10^{15}$ to 5.25×10^{15} electrons/m^2. The average value for the twenty-eight irregularities of excess ionization now becomes 1.62×10^{15} electrons $m/^2$ and the average value for the fourteen irregularities deficient in ionization becomes $.97 \times 10^{15}$ electrons/m^2, the new overall average becoming 1.41×10^{15} electrons/m^2.

Both ways for expressing the magnitude of these irregularities show that the regions of excess ionization have a greater magnitude than the regions deficient in ionization.

The magnitudes for each of the forty-two irregularities are listed in Table II.

2. Horizontal Dimensions of Irregularities

The horizontal dimension for the forty-two irregularities analyzed was measured as discussed in Chapter IV, Section 3. This value ranged from 38 to 117 km. The average dimension for the twenty-eight irregularities of excess ionization was 77 km and that for the fourteen irregularities deficient in ionization was 70 km. The overall average dimension was 75 km. Here again it can be seen that the regions deficient in ionization appear smaller than the regions of excess ionization.

The size of the measured dimensions is limited by the analysis techniques. The five or ten second averaging used in plotting the records governs the lower limit, while the condition that the dispersive doppler curves fairly well define an ambient line acts as an upper limit by restricting the irregularities to extend over no more than about one-third of a dispersive doppler record.

Comparison was made between the average dimension for irregularities which occurred on south to north satellite passes with that for those which occurred on north to south satellite passes with no significant difference found. This result may be an indication that the irregularities are circular in shape or elliptical with their elongation either in a north-south or east-west direction since, as stated earlier (Chapter III, Section 1), the

Table II

Magnitudes and Dimensions of Irregularities

Date	Time of peak Est	Percent of total electron content at peak	Electron content at peak $x10^{-15} m^{-2}$	Di-mensions km	Satel-lite direction
7- 7-61	1107:38	+.6	+.79	71	S-N
7- 7-61	1108:19	-.6	-.69	69	S-N
7- 8-61	1122:58	+1.6	+1.74	80	S-N
7-19-61	1745:44	+1.6	+1.08	63	N-S
8- 9-61	1210:33	+.9	+1.26	82	N-S
8- 9-61	1211:29	-1.6	-2.08	83	N-S
8- 9-61	1358:08	+.8	+1.12	72	N-S
8-21-61	0942:31	+.9	+1.46	58	N-S
8-21-61	0945:26	+1.6	+2.58	71	N-S
8-25-61	0856:00	+2.4	+3.72	73	N-S
10- 5-61	2328:35	+1.3	+.58	100	N-S
10- 5-61	2330:51	-1.4	-.61	99	N-S
10- 9-61	1333:46	+.3	+.67	39	S-N
10- 9-61	1334:37	+1.0	+1.93	69	S-N
10-19-61	2132:20	+1.9	+.86	82	N-S
10-19-61	2133:06	-1.4	-.63	91	N-S
10-20-61	1054:48	-.5	-.91	56	S-N
10-20-61	1055:30	+.4	+.70	65	S-N
10-24-61	1004:01	+2.9	+5.25	109	S-N
10-30-61	1848:27	-1.3	-.42	61	N-S

Table II continued.

Date	Time of peak EST	Percent of total electron content at peak	Electron content at peak $x10^{-15}$ m^{-2}	Di- mensions km	Satel- lite direction
10-30-61	1849:15	+3.2	+1.00	87	N-S
10-30-61	1849:57	-1.5	-.48	58	N-S
11-28-61	1135:50	+.7	+.95	51	N-S
11-28-61	1136:21	-.8	-1.12	52	N-S
12- 4-61	1115:52	-.5	-.62	50	S-N
12- 4-61	1116:15	+.5	+.64	38	S-N
1- 7-62	1649:57	+1.0	+2.89	115	S-N
1- 7-62	1835:34	+1.0	+2.14	117	S-N
1- 8-62	1703:29	-1.8	-.88	66	S-N
1- 9-62	1718:03	+2.4	+1.27	108	S-N
1-12-62	1614:40	+3.1	+1.61	92	S-N
1-18-62	1555:23	-.8	-.82	76	S-N
1-23-62	1332:38	+1.6	+1.43	69	S-N
1-27-62	1245:43	-.4	-.70	67	S-N
1-27-62	1246:16	+.4	+.76	47	S-N
2- 1-62	1209:40	+4.8	+5.31	67	S-N
2- 1-62	1210:20	-2.7	-2.74	67	S-N
2- 2-62	1224:15	+1.0	+1.10	92	S-N
2- 2-62	1225:21	+.9	+1.06	78	S-N
2- 3-62	2144:36	+1.7	+.18	60	N-S
2- 8-62	1017:43	-1.3	-.91	83	S-N
2- 8-62	1018:40	+1.8	+1.35	98	S-N

measured dimensions are parallel to the effective satellite ground track which, at 40° N latitude, makes an angle of approximately 28° either side with north depending upon the direction of the satellite pass.

The dimensions for the individual irregularities analyzed are listed in Table II.

3. Motion of Irregularities

When considering possible motion of these irregularities, it must be realized that for a given satellite observation the duration of usable data is about five minutes where each time on the record corresponds to a different ray path through the ionosphere. The next satellite pass, if visible to the same observer, occurs some hour and forty-three minutes later and is displaced about 26° to the west in longitude. Thus with the satellite traveling at an approximate horizontal velocity of 7 km/s, only a brief look at the ionosphere is obtained making direct detection of possible irregularity motion impossible through analysis of a single satellite record.

Comparison of the average dimension of the irregularities occurring on north to south satellite passes with that for south to north passes showed no apparent elongation in either direction. If motion did exist then either the motion was too small to detect or the motion was in a generally east-west direction and caused similar elongations in both satellite directions or the motion was in some

other direction and did cause an elongation such that the extent of the irregularity became too large to be considered within the restrictions discussed in the previous Section.

On 7 January 1962 dispersive doppler records were recorded for two consecutive satellite passes that showed definite similarity. Each record showed a single irregularity whose peak represented an excess of ionization equal to 1.0% of the total electron content. Assuming that it was the same irregularity on both records and that it was located around a height of 400 km, then its maximum velocity was 144 m/s in a generally north-west direction. This velocity falls within the range of values that have been measured for traveling disturbances.[12]

Figure 14 is a dispersive doppler plot that exhibits a cyclic behavior. This pass occurred on 3 July 1961 at about 1200 eastern standard time. It seems logical to suppose that a cyclic effect as seen here is caused by some sort of cyclic disturbance such as a traveling wave. Since the satellite technique used is insensitive to the height distribution of the electrons, a traveling wave that merely caused a deformation of the contours of electron density would not produce the effect seen on Figure 14. To do this would take some form of horizontal compressional wave.

Since the evidence for motion is indirect, consideration must be given to the case where the irregularity represents a local disturbance which does not undergo any significant horizontal translation. Experimental evidence suggests vertical motion in the

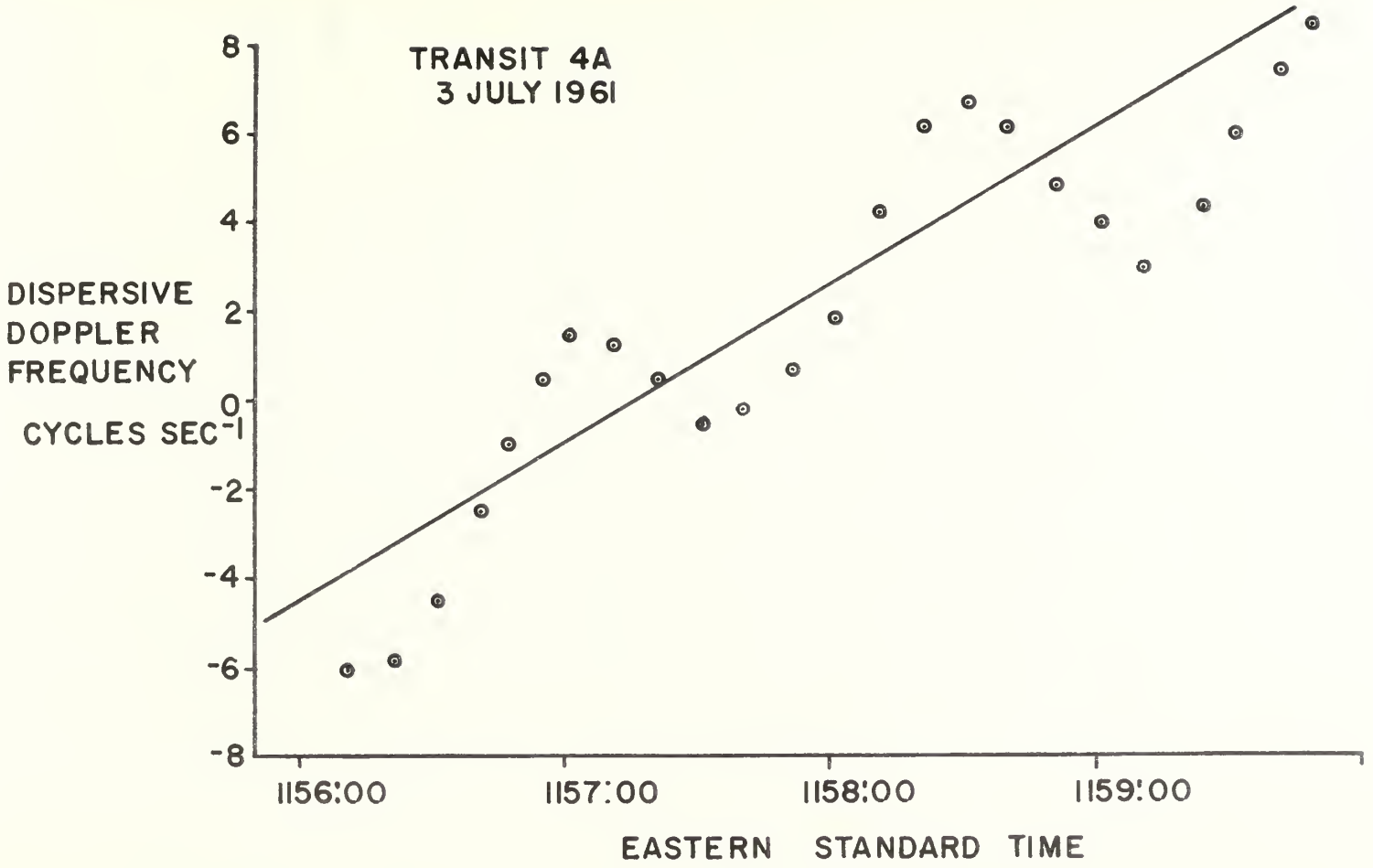

DISPERSIVE DOPPLER PLOT SHOWING POSSIBLE CYCLIC IRREGULARITY

FIGURE 14

ionosphere possibly caused by electromagnetic forces, diffusion, and temperature changes.[1] If these movements are not uniform then the possibility exists that the quasi-equilibrium condition, in which the constituents exist, could be disturbed in such a way as to form regions that have increased or decreased production or loss rates. Any such irregularity, however, would not remain static because of the diffusion properties in the ionosphere. At F region heights the time necessary for the electron-positive ion plasma to attain diffusive equilibrium is of the order of one hour.[1] Around mid-latitudes, at which this experiment was conducted, vertical diffusion predominates (Chapter I, Section 1). Since, as mentioned above, a single satellite observation can not provide direct evidence of irregularity motion, then neither can it establish that there is no motion. Further, no information regarding the duration of these irregularities can be obtained since consecutive satellite passes are widely separated in longitude.

4. Height of Irregularities

As previously mentioned, the satellite techniques used here are insensitive to the height distribution of the electrons and thereby do not give any height information on the irregularities.

Work was carried out, however, using spaced stations in an attempt to determine the height of an irregularity by triangulation. The second station used was the Applied Physics Laboratory located at 39.16° N and 76.90° W. The distance between the two stations is

about 200 km and the base line drawn between the two lies approximately parallel to the ground track of the north to south satellite passes. This work was commenced on 5 January 1962 and did not yield any results. North to south satellite passes had to be used, since for these the two surfaces, generated by the two rays from the observers to the satellite, were approximately coincident meaning that both observers would be looking at the same part of the irregularity. These passes occurred during the daytime during the month of February. Unfortunately there were no well defined irregularities for this period that could be defined on the records from both stations. The next time north to south satellite passes occur during the day would be too late for inclusion in this thesis. It should also be noted that due to a different recording technique the dispersive doppler records from the Applied Physics Laboratory had about one-sixth the resolution of the records taken at University Park. This further hindered identification.

Indirect evidence as to the height of these irregularities can be obtained from consideration of the comments made in Section 1 of this Chapter as regards the magnitude of these irregularities as expressed in a percent of the total electron content. If it is assumed that the irregularities are restricted in height, then in order to keep the percent of local electron density contained within the anomalies a minimum, the irregularities must be located around the height of maximum density, the peak of the F2 layer. Because of diffusion, however, this height restriction would not be expected to be of long duration.

CHAPTER VI

SUMMARY AND CONCLUSIONS

A method has been developed for identifying large scale ionospheric irregularities on dispersive doppler records from earth satellite Transit 4A (1961 Omicron One). This method was applied to data recorded at University Park, Pennsylvania over the nine-month period from 29 June 1961 to 10 April 1962. During this time, out of 501 satellite dispersive doppler records recorded, 90 exhibited evidence of irregularities of which some represented regions of excess ionization while others represented regions deficient in ionization. These irregularities can occur at any time of day.

The instrumentation used for receiving, recording, and analyzing satellite dispersive doppler information was described briefly.

A technique of analysis was developed and applied to twenty-seven dispersive doppler records, representing a total of forty-two irregularities, to determine the characteristics of these irregularities. The results of this showed that the average magnitude of the irregularities represented 1.4% of the total columnar electron content in the ionosphere and that their average dimension was about 75 km, assuming the irregularities to be situated at a height of 400 km. A comparison made between irregularities of excess ionization and irregularities deficient in ionization showed that the former had greater magnitudes and dimensions on the average than the latter.

No definite conclusions could be drawn regarding whether or not the irregularities traveled through the ionosphere, however, some indirect evidence showed the possibility that the irregularities were the result of a horizontal compressional traveling disturbance.

Another question that could not be solved directly was the one of height. Although spaced stations were used for triangulation, no results were obtained. By assuming, however, that the extent of the irregularities is restricted in height, it can be concluded that the irregularities are most likely situated around the peak of the F2 layer. Such irregularities could not remain restricted for long because of the presence of diffusion.

CHAPTER VII

SUGGESTIONS FOR FURTHER INVESTIGATION

Although the data reported on covered a period of nine months, the number of analyzable records with irregularities was insufficient to establish any possible diurnal or seasonal trends. Continued analysis of irregularities is therefore needed.

In order to answer the question of height, more spaced stations should be established such that both south-going and north-going satellite passes could be used for triangulation purposes. Also all the stations should have the same receiving and recording equipment to reduce the problems of irregularity identification encountered in this experiment.

An experiment should be conducted using either a fixed frequency vertical sounder, operating at 5.8 mc/s and at somewhat lower frequency at night, or a swept frequency sounder, using a range of from 1 to 15 mc/s, in conjunction with the techniques described in Chapter III. In so doing it could be determined if any possible correlation exists between the type of irregularities analyzed in this experiment and the Munro type traveling disturbances.[18]

BIBLIOGRAPHY

[1]Ratcliffe, J. A., Physics of the Upper Atmosphere, Pergamon Press (1960).

[2]Johnson, F. S., Satellite Environment Handbook, Stanford University Press (1961).

[3]Berning, W. W., "A Sounding Rocket Measurement of Electron Densities to 1500 Kilometers", Journal of Geophysical Research, 65, 9 (1960).

[4]Schmerling, E. R., Scientific Report No. 94, Ionosphere Research Laboratory, The Pennsylvania State University (1957).

[5]Hok, G., Spencer, N. W. and Dow, W. G., "Dynamic Probe Measurements in the Ionosphere", Journal of Geophysical Research, 58, 235 (1953).

[6]Jackson, J. E. and Kane, J. A., "Performance of an RF Impedance Probe in the Ionosphere", Journal of Geophysical Research, 65, 2209 (1960).

[7]Garriott, O. K., "The Determination of Ionospheric Electron Content and Distribution from Satellite Observations. Parts 1 and 2", Journal of Geophysical Research, 65, 4 (1960).

[8]Bowles, K. L., "Incoherent Scattering by Free Electrons, as a Technique for Studying the Ionosphere and Exosphere", Journal of Research of NBS, Part D (1960).

[9]Gordon, W. E., "Incoherent Scattering of Radio Waves by Free Electrons with Special Reference to the Ionosphere", Proceedings of the Institute of Radio Engineers, 46, 1824 (1958).

[10]Hewish, A., "The Diffraction of Galactic Radio Waves as a Method of Investigating the Irregular Structure of the Ionosphere", Proceedings of the Royal Society, A214, 494 (1952).

[11]Martyn, D. F., "The Normal F Region of the Ionosphere", Proceedings of the Institute of Radio Engineers, 47, 147 (1959).

[12]Munro, G. H., "Traveling Disturbances of the Ionosphere", Proceedings of the Royal Society, A202, 208 (1950).

[13]Heisler, L. H., "Anomalies in Ionosonde Records due to Traveling Ionospheric Disturbances", Australian Journal of Physics, 11, 79 (1958).

[14]Chan, K. L. and Villard, O. G. Jr., "Observations of Large-Scale Traveling Ionospheric Disturbances by Spaced-Path High-Frequency Instantaneous-Frequency Measurements", Journal of Geophysical Research, 67, 973 (1962).

[15]Hines, C. O., "Electron Resonance in Ionospheric Waves", Journal of Atmospheric and Terrestial Physics, 9, 56 (1956).

[16]Ratcliffe, J. A. The Magneto Ionic Theory and Its Application to the Ionosphere, Cambridge University Press (1959).

[17]Ross, W. J., "The Determination of Ionospheric Electron Content from Satellite Doppler Measurements", Journal of Geophysical Research, 65, 2607 (1960).

[18]Munro, G. H., "Traveling Ionospheric Disturbances in the F Region", Australian Journal of Physics, 11, 91 (1958).